

IMPACT OF TYPE IA SUPERNOVA EJECTA ON A HELIUM-STAR BINARY COMPANION

KUO-CHUAN PAN¹, PAUL M. RICKER¹ AND RONALD E. TAAM^{2,3}

¹Department of Astronomy, University of Illinois at Urbana-Champaign, 1002 W. Green Street, Urbana, IL 61801; kpan2@illinois.edu, pmricker@illinois.edu

²Department of Physics and Astronomy, Northwestern University, 2131 Tech Drive, Evanston, IL 60208; taam@tonic.astro.northwestern.edu and

³Academia Sinica Institute of Astronomy and Astrophysics, P.O. Box 23-141, Taipei 10617, Taiwan

Draft version October 29, 2018

ABSTRACT

The impact of Type Ia supernova ejecta on a helium-star companion is investigated via high-resolution, two-dimensional hydrodynamic simulations. For a range of helium-star models and initial binary separations it is found that the mass unbound in the interaction, δM_{ub} , is related to the initial binary separation, a , by a power law of the form $\delta M_{\text{ub}} \propto a^m$. This power-law index is found to vary from -3.1 to -4.0 , depending on the mass of the helium star. The small range of this index brackets values found previously for hydrogen-rich companions, suggesting that the dependence of the unbound mass on orbital separation is not strongly sensitive to the nature of the binary companion. The kick velocity is also related to the initial binary separation by a power law with an index in a range from -2.7 to -3.3 , but the power-law index differs from those found in previous studies for hydrogen-rich companions. The space motion of the companion after the supernova is dominated by its orbital velocity in the pre-supernova binary system. The level of Ni/Fe contamination of the companion resulting from the passage of the supernova ejecta is difficult to estimate, but an upper limit on the mass of bound nickel is found to be $\sim 5 \times 10^{-4} M_{\odot}$.

Subject headings: binaries: close — supernovae: general — methods: numerical

1. INTRODUCTION

Type Ia supernovae (SNe Ia) are among the most catastrophic and energetic events in the Universe. Because they are so luminous, and because their light-curve shapes and absolute magnitudes are correlated, SNe Ia can be used as “standardizable candles” in measuring the distances to remote galaxies, allowing constraints to be placed on key cosmological parameters (Branch & Tammann 1992; Riess 1996). SNe Ia also play a major role in galactic chemical evolution via their energy and metal input to the interstellar medium. Thus, the nature of their progenitor systems and the physical origin of variations in their properties are fundamental problems of great interest (Domínguez et al. 2001; Howell et al. 2007).

Most work on progenitor models for SNe Ia has focused on two general classes of systems. The single-degenerate scenario involves a CO white dwarf (WD) accreting matter from a non-compact stellar binary companion, eventually becoming unstable to explosive nuclear burning (Whelan & Iben 1973; Nomoto 1982). On the other hand, the double-degenerate scenario involves the merger of two CO WDs whose orbital decay results from the loss of angular momentum due to gravitational wave emission (Iben & Tutukov 1984; Webbink 1984).

Single-degenerate models require that the rate of mass accretion be such that the WD avoid a nova explosion. For a high accumulation efficiency, stable burning on the WD is required, but this burning phase occurs in a fairly narrow range above $10^{-7} M_{\odot} \text{ yr}^{-1}$. For rates greater than this range, a wind from the WD develops that limits the accretion efficiency (Nomoto 1982; Hachisu et al. 1996; Ivanova & Taam 2004), making it difficult to explain the observed low-redshift SN Ia rate

of $3 \times 10^{-5} \text{ Mpc}^{-3} \text{ yr}^{-1}$ (Mannucci 2005) using single-degenerate progenitors alone. Although the predicted and observed numbers of double-degenerate systems are sufficient to explain the observed rate (Nelemans et al. 2001; Napiwotzki et al. 2001, 2002), it is more likely that WD-WD mergers lead to the production of an ONeMg WD followed by accretion-induced collapse to a neutron star (Nomoto & Iben 1985; Ivanova & Taam 2004; Dessart et al. 2006; Wickramasinghe et al. 2009). Moreover, the wide range of total WD masses suggests that double-degenerate models should exhibit much more heterogeneity than is observed in SN Ia light curves (Goldhaber et al. 2001; Knop et al. 2003).

Maoz (2008) analyzed the observed SN Ia rate for assumed initial mass functions (IMF) and concluded that almost all intermediate-mass close binary systems in the range $3 - 8 M_{\odot}$ should evolve to the SN Ia stage. This result allows for a wide range of possibilities for SN Ia progenitor systems. Furthermore, observations of the SN Ia rate as a function of redshift suggest the need for a two-component model for the delay time distribution (DTD). (The delay time is the interval between a star’s arrival on the zero-age main sequence and its destruction in an SN Ia.) Scannapieco & Bildsten (2005) and Mannucci et al. (2006) found that the observations can be fit with a short-delay-time population having delays of $\sim 10^8 \text{ yr}$ and a long-delay-time population having delays of $3 - 4 \text{ Gyr}$.

To provide an explanation for the two populations suggested by the observed SN Ia rate, several pre-supernova progenitor models have been investigated. The long-delay-time population can be understood in terms of progenitor systems characterized by a main-sequence-like companion in the MS-WD channel

(Hachisu et al. 2008b) and/or by a red giant in the RG-WD channel (Hachisu et al. 1996, 1999a,b, 2008a). In contrast, the short-delay-time population may consist of systems characterized by a massive MS star in the MS-WD channel or by a He star in the He-WD channel (Waldman et al. 2008; Wang et al. 2009a,b; Wang & Han 2010; Meng & Yang 2009).

Numerically, Marietta et al. (2000) explored the influence of the supernova explosion on the companion star in the single-degenerate channel with hydrogen-rich stars consisting of red giants, subgiants, and main-sequence stars using two-dimensional Eulerian hydrodynamics simulations. They found that significant quantities of hydrogen would be unbound from the companion star in each case (15% of the envelope for main-sequence and subgiant cases, and 98% of the red giant envelope), in conflict with observational upper limits on the amount of hydrogen inferred from SN Ia spectra (Mattila et al. 2005; Leonard 2007).

A more recent hydrodynamical study by Pakmor et al. (2008) reexamined the main-sequence simulation of Marietta et al. (2000) using a three-dimensional smoothed particle hydrodynamics (SPH) simulation. In contrast to Marietta et al., Pakmor et al. adopted the structure for the companion star based on the binary evolutionary models of Ivanova & Taam (2004), which yielded more compact main-sequence-like companions. As a consequence, Pakmor et al. found a tenfold reduction in the amount of unbound mass compared with Marietta et al., bringing the prediction of the amount of unbound hydrogen-rich material into agreement with the observational upper limits.

In a complementary analytical study, Kasen (2010) investigated the radiation emitted by the collision of SN Ia ejecta with a red giant, finding that the light curve should depend on the viewing angle. This result was attributed to the fact that the gas is more transparent in the region shadowed by the companion star. This suggests the possibility that the secondary star may be detectable in future observational studies.

These previous simulations of the effect of a supernova impact on a companion star have been carried out only for models applicable to the long-delay-time population of SN Ia. In contrast, Wang et al. (2009a,b) suggest a progenitor binary model based upon a helium-star channel for the short-delay-time population. Using a binary evolution model, for this channel they find a SN Ia birthrate $\sim 3 \times 10^{-4} \text{ yr}^{-1}$ and a corresponding delay time of $\sim 4.5 \times 10^7 \text{ yr}$ to $\sim 1.4 \times 10^8 \text{ yr}$ (Wang & Han 2010). The latter delay time is consistent with that estimated from observations for the short-delay-time population by Scannapieco & Bildsten (2005), Mannucci et al. (2006), and Aubourg et al. (2008).

In this paper we report the results of Eulerian hydrodynamics simulations of the impact of SN Ia ejecta on companion stars for the single-degenerate helium-star channel. In the next section, the assumptions underlying our study, the construction of the initial model, and the numerical method are described. Our numerical results for a range of helium-star models and orbital separations are reported in § 3 and their implications are discussed in § 4. In the final section, we summarize our results and make some concluding remarks.

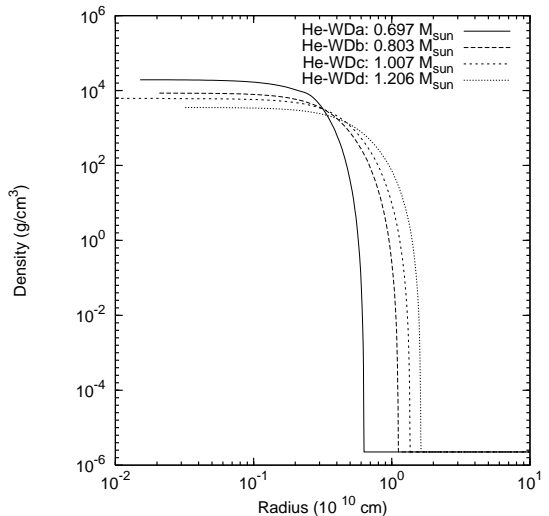


FIG. 1.— Density profiles of the helium-star models at the onset of the supernova explosion, as obtained using the one-dimensional stellar evolution code.

2. NUMERICAL METHODS AND MODELS

2.1. Numerical codes

For our hydrodynamical simulations we used FLASH version 3 (Fryxell et al. 2000; Dubey et al. 2008). FLASH is a parallel, multi-dimensional hydrodynamics code based on block-structured adaptive mesh refinement (AMR). To solve the Euler equations on the AMR grid, we used the piecewise parabolic method (Colella & Woodward 1984) with modifications to handle nonideal equations of state (Colella & Glaz 1985). The equation of state used is interpolated from a precomputed table of the Helmholtz free energy. It includes contributions from radiation, completely ionized nuclei, and degenerate electrons and positrons (Timmes & Swesty 2000) for an optically thick mixture of gas and radiation in local thermodynamic equilibrium.

The helium-star models used in our simulations were generated using a one-dimensional stellar evolution code (Eggleton 1971, 1972, 1973). We simulated four helium-star models with initial masses equal to 1.25, 1.35, 1.4, and $1.8 M_{\odot}$. To evolve the helium-star models to the onset of the supernova explosion, an artificial constant mass loss rate was adopted such that the evolution time and final helium star masses were consistent with the detailed binary evolutionary models of Wang et al. (2009b). The resulting models are summarized in Table 1. The density profiles of the helium-star models at the onset of the supernova explosion are illustrated in Figure 1. It can be seen that the more massive models are characterized by larger radii and less compact cores.

2.2. Initial setup

Since the speed of the ejecta in a SN Ia ($\lesssim 10^4 \text{ km s}^{-1}$) is much higher than the orbital speed of the helium star ($\lesssim 10^3 \text{ km s}^{-1}$) in a binary system, we ignore the orbital motion in the first approximation and consider a 2D axisymmetric geometry. The simulation domain is described using cylindrical coordinates (r, z) , with the z -axis defined as the direction along the line connecting the centers of the white dwarf and the helium star. We consider a simulation domain with a size equal to fifteen

TABLE 1
HELIUM-STAR MODELS.

Model	Mass (M_{\odot})	Radius (10^{10} cm)	Evolution time (yr)	m_{ub}^{a}	C_{ub}^{a}	$m_{\text{kick}}^{\text{b}}$	$C_{\text{kick}}^{\text{b}}$
He-WDa	0.697	0.63	9.2×10^6	-4.01	1.42	-3.28	4150
He-WDb	0.803	1.10	5.2×10^5	-3.13	0.70	-2.90	2413
He-WDc	1.007	1.35	2.2×10^5	-3.48	1.17	-3.18	2703
He-WDd	1.206	1.63	6.1×10^4	-3.51	1.35	-2.71	1729

^aThe entries for the power-law index, m_{ub} , and power-law constant, C_{ub} , refer to the power-law fit to unbound mass versus orbital separation described in eq. 1.

^bThe entries for the power-law index, m_{kick} , and power-law constant, C_{kick} , refer to the power-law fit to kick velocity versus orbital separation described in eq. 2.

times the radius of the helium star (R_{He}) in the radial direction and $30 R_{\text{He}}$ in the axial direction. For convenience, the helium star is located at the origin of the coordinate grid.

To simplify the problem, the composition of the one-dimensional helium-star model was taken to be a uniform distribution of 98% helium and 2% carbon by mass when used in FLASH. This simplification leads to an error of $\lesssim 2\%$ in the composition and $\lesssim 4\%$ in the radius for the lowest-mass helium-star model. To initialize the two-dimensional FLASH simulations, we first interpolated the one-dimensional model onto the FLASH grid using up to twelve levels of refinement based on the magnitudes of the second derivatives of gas density and pressure. With each block containing 8×16 zones, the equivalent uniform-grid resolution is thus $16,384 \times 32,768$. For model He-WDc, the minimum zone spacing at this level of refinement corresponds to 1.22×10^7 cm. Within the helium star, a minimum of nine levels of refinement was used (corresponding to a maximum zone spacing of 9.76×10^7 cm for model He-WDc). Because the surface of the helium star is characterized by a very steep density gradient, we established a sharp cutoff radius to avoid pressure errors at the surface. The cutoff radius was chosen such that each density drop of one order of magnitude is resolved by at least three zones in the surface region (we have more than 40 zones per order of magnitude in the core region). Outside the cutoff radius, the density was set to an ambient value of 2.25×10^{-6} g cm $^{-3}$, and the pressure was set to the value of the helium-star model pressure profile at the cutoff radius. The simulations, therefore, employed the same ambient density but somewhat different ambient pressures. The composition of the ambient gas in each case was taken to be pure hydrogen.

The helium-star model was relaxed on the Eulerian grid by artificially damping the momentum for a period of time greater than about thirty times the average dynamical time scale. During this time the damping factor was smoothly increased from 0.7 to 0.99, ensuring that the Mach number in the helium-star interior was always smaller than 0.01. Once this process was complete, the damping was removed and the gas velocity was reset to zero. The supernova explosion was then introduced to the grid. During the subsequent evolution, we allowed second-derivative refinement up to seven levels everywhere except in two regions: within the helium star at any time, and in a region surrounding the supernova explosion for the first 150 seconds, we required

nine levels of refinement (equivalent to a resolution of 2048×4096 for a uniform grid with a minimum zone spacing of 9.77×10^7 cm in model He-WDc). The extra refinement for the supernova region reduces the influence of grid artifacts on the developing explosion. The explosion itself was introduced by creating a spherical region of high-density and high-temperature gas with radius equal to twenty times the minimum zone spacing at nine levels of refinement. Each run used this “7/9” refinement pattern except for one model that was also run at 6/8, 8/10, 9/11, and 10/12 to study convergence (see § 3.3).

The Type Ia supernova model used is the W7 model described by Nomoto et al. (1984), which corresponds to a carbon deflagration in an accreting CO WD. The initial carbon deflagration is assumed to develop in the central regions of the white dwarf and is then followed by a detonation. This one-dimensional model provides a good fit to observed light curves and can be approximated by a white dwarf of mass $M_{\text{wd}} = 1.378 M_{\odot}$, total explosion energy $E_{\text{sn}} = 1.233 \times 10^{51}$ erg, and average speed $v_{\text{sn}} = 8.527 \times 10^3$ km s $^{-1}$. This mass is uniformly distributed within the spherical perturbation used to start the calculation. The velocity inside the perturbation is taken to be radially outward and uniform in magnitude; the internal energy is set using v_{sn} and E_{sn} . We assume the ejecta to be entirely ^{56}Ni and use this fluid component as a tracer for the ejecta. The mass of the supernova ejecta creates a potential perturbation that changes the equilibrium state of the helium star. However, in all of our models the radius of the helium star is smaller than the Roche lobe radius, and the timescale on which the equilibrium is upset by the supernova shock, $\sim a/v_{\text{sn}}$ (a is the initial binary separation), is shorter than the average dynamical timescale in the helium star. Thus we expect that the altered pre-supernova potential should not have a significant effect on the structure of our models. However, because the orbital motion is ignored in this study, the gravitational force from the supernova material will attract the helium star and cause a small velocity perturbation toward the supernova material. This velocity perturbation can be comparable to the kick velocity of the helium star after supernova impact but is much smaller than the ejecta speed.

3. RESULTS

In this section, we describe the numerical results for the standard case, model He-WDc, and explore the dependence of the system’s evolution on the mass of the helium-star companion and the initial binary orbital separation a . To determine the sensitivity of the results to

the numerical resolution, we also describe a convergence test.

3.1. Qualitative description of evolution

Immediately after the onset of the supernova explosion, a double shock structure is formed as the ejecta interact with the surrounding medium (label A in Figure 2; the figure illustrates the evolution of a simulation with initial binary separation of 4×10^{10} cm, $\sim 3 R_{\text{He}}$, and 9/11 levels of refinement). A forward shock expands outward into the ambient medium, and a reverse shock propagates inward (in Lagrangian coordinates). The two shocks are separated by a contact discontinuity (Dwarkadas & Chevalier 1998). During this free expansion phase, the swept-up ambient medium has very little effect, except for the development of an instability at the contact discontinuity. This instability is unimportant in affecting the helium star, as it is seeded by a numerical grid effect and is Rayleigh-Taylor unstable (label A) (Dwarkadas 2000). The expansion of the ejecta leaves behind an extremely low-density region at the center of the supernova (label a) that is prone to numerical grid effects which become visible due to the color scale; these are smoothed out later by the reflected shock (label C). The SN ejecta reach the companion at $t \sim a/v_{\text{sn}} \sim 50$ seconds, at which time a bow shock forms at the leading surface of the companion, making an angle of $\sim 40^\circ$ with respect to the z -axis. This can be seen in the upper-left panel of Figure 2 (label B)¹. As the bow shock propagates further, the shearing of gas in conjunction with the action of gravity due to the helium star causes distortions in the bow shock structure. After the impact of the ejecta on the helium star, ejecta material begins to reflect and refill the central supernova region (label C in Figure 2). As a result of the mixing beginning at ~ 100 seconds associated with the Kelvin-Helmholtz and Rayleigh-Taylor instabilities in the envelope of the helium star (label D in Figure 2), the bow shock breaks up and is divided into a curved shock and a straight shock that makes an angle of $\sim 40^\circ$ with the z -axis (label B in the upper-right panel of Figure 2). The instabilities continue to develop between ~ 100 s and ~ 600 s as the mixing region moves away from the helium-star envelope (lower-left panel of Figure 2). At around 100 s, the shock propagates to the center of the helium star, leading to the pulsation of the helium star. Smooth shocks (label E in Figure 2) are continually generated by the oscillation of the helium star after ~ 600 s. Radial shocks (label F in Figure 2), which result from the interaction of shocks on the rear side of the helium star, sweep around the helium star (lower-right panel of Figure 2). As the helium star evolves further, its density profile becomes smoother, approaching a new equilibrium state. Qualitatively, our results are similar to results reported by Marietta et al. (2000) and Pakmor et al. (2008) for the main-sequence case, but with a more compact companion and smaller binary separation. As a result of the asymmetric interaction, a small kick velocity, $v_{\text{kick}} \sim 85 \text{ km s}^{-1}$, is imparted to the helium star.

3.2. Parameter survey

We conducted a parameter survey to explore the dependence of the numerical results on the binary progenitor’s properties. Note that Wang et al. (2009b) determined the orbital period, and thus the orbital separation, at the onset of the supernova explosion, for each choice of helium star and white dwarf. In our study we do not follow the binary evolution up to the explosion, so the Roche-lobe radii of Wang et al.’s models are actually larger than the radii of our helium-star models. Therefore, in addition to varying the mass of the helium star, we also vary the binary separation in order to determine the effect of this parameter.

Figure 3 shows the typical time evolution of the amount of mass removed from the helium star (defined as total unbound helium mass) by the SN ejecta. The first peak occurs at the initial impact (~ 30 s), but then some gas becomes bound again after the ejecta pass through the helium star. At ~ 80 – 100 seconds, a second peak develops which is associated with the effect of the reverse shock. Lastly, a third peak at ~ 500 seconds occurs when the compressed helium star relaxes and starts to oscillate. After 1,500 seconds, the amount of unbound mass reaches an approximately steady value. The final unbound mass is thus calculated for a given initial binary separation and helium-star model by averaging the unbound mass values computed for several time steps at this late stage.

Figures 4 and 5 show the final unbound mass and helium-star kick velocity (defined as the center-of-mass velocity of the final bound helium) as functions of the binary separation in our simulations. We include 14% error bars in Figure 4 and Figure 5 based on the results of our convergence test (§ 3.3). We find that the unbound mass can be fit by the relation

$$\delta M_{\text{ub}} = C_{\text{ub}} a^{m_{\text{ub}}} M_{\odot}, \quad (1)$$

where a is the orbital separation, m_{ub} is the power-law index, and the constant C_{ub} depends only on the helium-star model (see Table 1). For comparison, we also plot the power-law relation with index -3.49 found by Pakmor et al. (2008) and the data from Marietta et al. (2000) for main-sequence companions (consistent with an index of -3.14). The power-law indices for our helium-star companions vary in a small range and bracket their results, suggesting that the index may be insensitive to the evolutionary state of the companion. The normalization of the above relation does appear to be sensitive to the nature of the companion star.

The kick velocity of the helium star is calculated by differencing the center-of-mass positions in the z -direction at different timesteps. Alternatively, it can be determined by dividing the total bound helium star momentum by the total bound helium star mass. Both methods yield the same kick velocity. To smooth out short-term fluctuations, we average the center-of-mass positions for every ten steps, then determine the kick velocity by numerical differentiation of these averaged values. The helium star is initially accelerated by the SN ejecta with an acceleration $\sim GM_{\text{wd}}/a^2$ for a time $\sim a/v_{\text{sn}}$, and then it is kicked by the SN ejecta during the initial impact. During the initial impact, the kick velocity varies dramatically. However, after $\sim 1,000$ seconds, these variations decay. Thus, we define the kick velocity by using the difference between the final averaged velocity and the

¹ Movies are available at <http://sipapu.astro.illinois.edu/foswiki/bin/view/Main/BinarySupernovae>

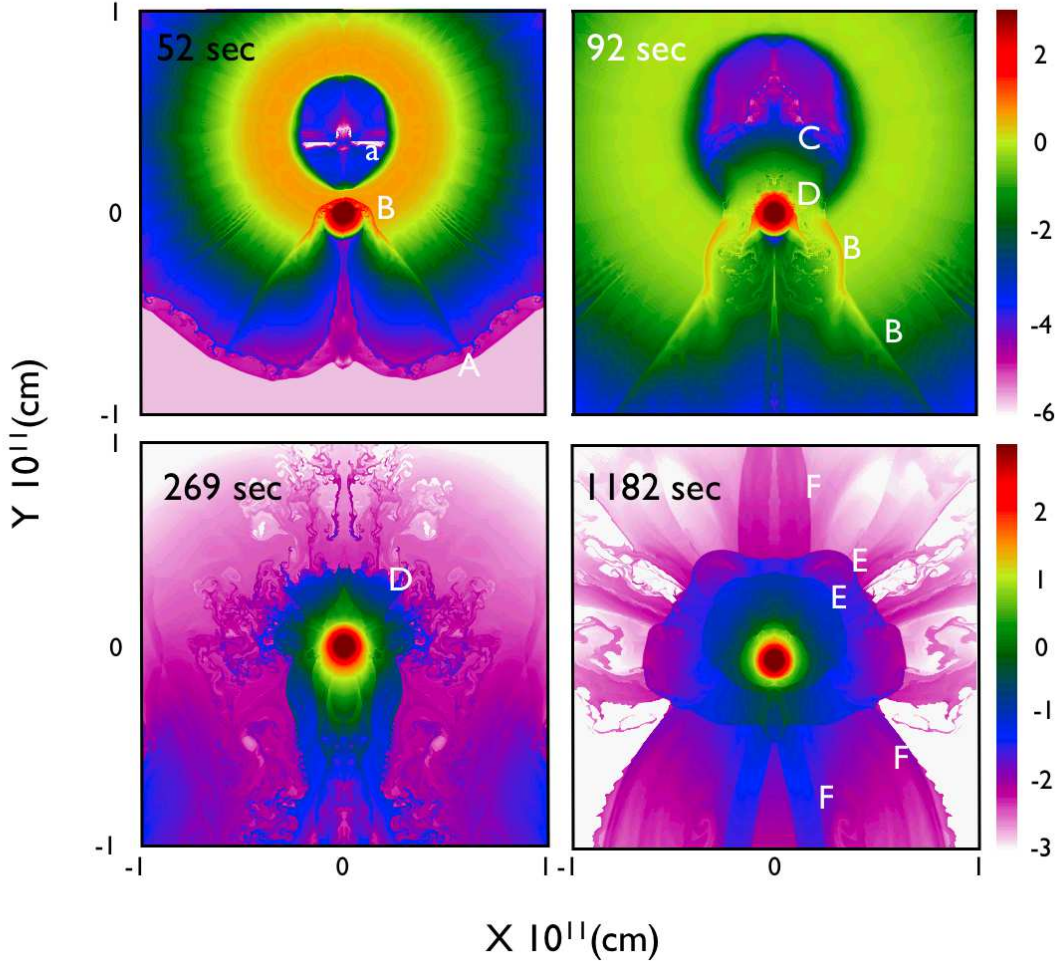


FIG. 2.— The density distribution for model He-WDc (see Table 1) with initial binary separation of 4×10^{10} cm. Each frame shows a portion of the domain spanning 10^{11} cm. Letters refer to features described in the text. The color scale indicates the logarithm of the gas density in g cm^{-3} .

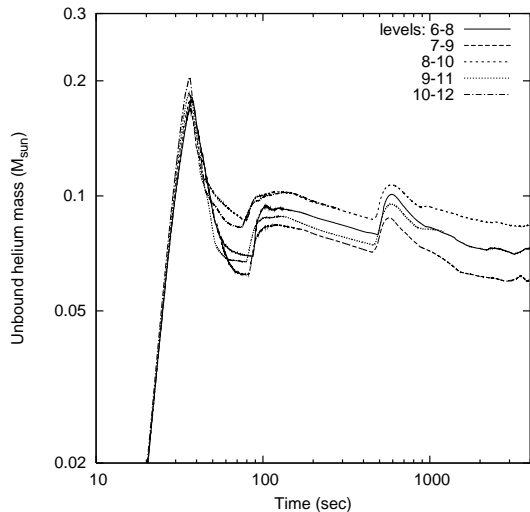


FIG. 3.— Unbound helium mass versus simulation time using different levels of refinement for the He-WDc model (see Table 1) with initial separation 3×10^{10} cm. (Note: the 10/12 run was very expensive and was carried out only up to 292 s.)

maximum velocity just before the impact of the SN ejecta (the exact time range to average the final velocity varies

from run to run and covers the entire period of “smooth” variation in the kick velocity). Figure 5 shows the kick velocity for the different helium-star models and initial binary separations. For initial binary separations larger than $4 R_{\text{He}}$ the kick velocity could not be adequately determined, because the perturbed velocity from the SN is larger than the kick velocity at larger separations. As obtained by Pakmor et al. (2008) and Meng et al. (2007), a power-law relation is also found in our simulation and can be fitted by the relation

$$v_{\text{kick}} = C_{\text{kick}} a^{m_{\text{kick}}}, \quad (2)$$

where v_{kick} is the kick velocity, m_{kick} is the power-law index, and the constant C_{kick} depends only on the helium-star model (see Table 1). However, unlike the situation for the final unbound mass, the slope is very different from that found in the case of main-sequence companions ($m_{\text{kick}} = -1.45$ in Pakmor et al. (2008), and $m_{\text{kick}} = -1.26$ in Marietta et al. (2000)) (see §4.1).

3.3. Convergence test

In order to determine the robustness of our numerical results, we performed a convergence test for model He-WDc. We carried out simulations with the same ini-

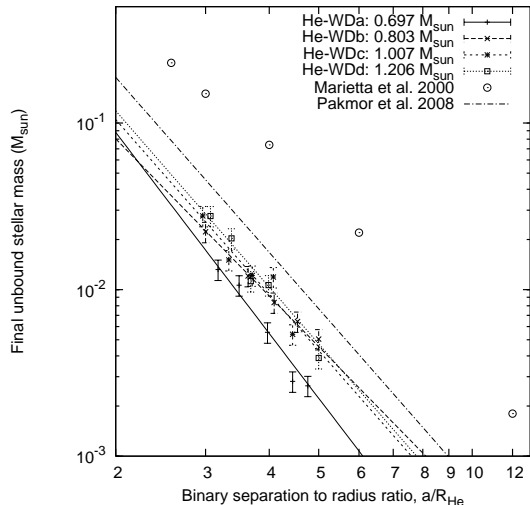


FIG. 4.— Final unbound stellar mass versus binary separation for different helium-star models. The separation is expressed in units of the helium-star radius. The lines show power-law relations from numerical simulations for different helium-star models (Table 1). Error bars are based on the 14% error determined in our convergence test. The dash-dot line is the fitted curve provided by Pakmor et al. (2008) and the circles are the data from Marietta et al. (2000).

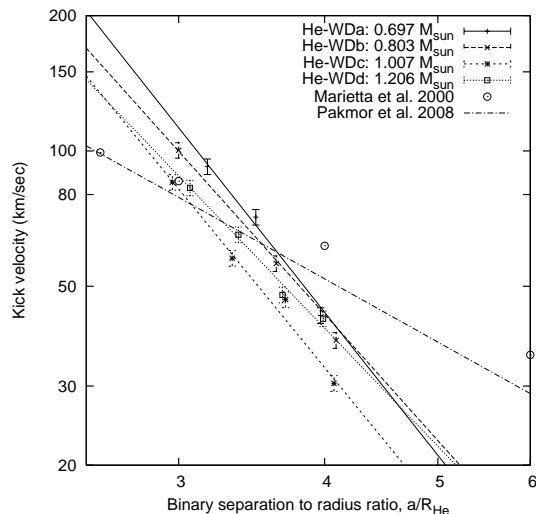


FIG. 5.— Similar to Figure 4 but for kick velocity versus binary separation for different helium-star models. Error bars are based on the 4% error determined in our convergence test.

tial binary separation ($a = 3 \times 10^{10}$ cm) but several different maximum AMR levels, computing the amount of unbound mass in each run as a function of time. The unbound mass is found by calculating the difference between the initial helium-star mass and the measured total bound helium mass at each step. The total bound helium mass is the sum of the helium masses in all zones for which the total energy is negative. The results, which are plotted in Figure 3, show that the final unbound mass lies in the range between the 8/10 and 10/12 runs. The unbound mass is sensitive to the level of turbulence that occurs near the surface of the helium star, particularly for resolutions higher than 8/10 (see Fig. 6), so rather than observing normal convergence behavior, we find that the unbound mass for runs with different resolutions fluctu-

ates within a small range of values. Similar behavior is also found with other initial binary separations. Thus, the difference in unbound helium mass between the 8/10 and 9/11 calculations ($\sim 0.01 M_{\odot}$) is used to estimate a relative error. Because the unbound helium mass reaches an approximately steady value at late times, this difference suggests an estimate of about $\pm 14\%$ for the relative error in our runs, since it is not clear whether the 7/9 run is always the lower limit of unbound mass for different models or different separations. Similar analysis gives a $\pm 4\%$ relative error in kick velocity. To allow for a feasible parameter study, a resolution of 7/9 levels was chosen for the whole suite of twenty runs.

4. DISCUSSION

4.1. Stripped and ablated mass

The impact of SN Ia ejecta on a helium-star companion is not as dramatic as for a main-sequence or red-giant companion like those considered by Marietta et al. (2000) because helium-star companions are more compact. This can be seen in Figure 7, which shows the gas pressure profile along the z -axis at several different times during the evolution of model He-WDc with an initial binary separation of 4×10^{10} cm. While the pressure immediately behind the ejecta shock front is initially $\sim 10^{21}$ dyne cm^{-2} , by the time the front reaches the helium star it has dropped to $\sim 10^{13}$ dyne cm^{-2} . The shock is considerably weakened by the time it reaches the deep interior of the star. As a result, the amount of unbound mass is much lower than in the case for main-sequence companions for a given ratio of separation to radius, $a/R \sim 3$, even though the helium-star channel is characterized by smaller binary separations.

If we assume that the WD accretion and subsequent explosion in our models are driven by Roche lobe overflow (RLOF), the physically appropriate initial binary separations for models *a* to *d* should be 3.11, 3.00, 2.84, and 2.72 times R_{He} . The total unbound helium masses for these models at these radii (Figure 4) are $\sim 1-3\%$ of the initial helium-star masses, which is consistent with the suggested upper limit of $\sim 0.01 M_{\odot}$ determined by Leonard (2007) from observations.

The unbinding of mass from the helium star results either from ablation (heating) or from stripping (momentum transfer) by the ejecta. To estimate the relative contribution of these processes, we examined the mixing of nickel in the helium-star material. Because stripping involves the physical displacement of gas from the helium star by the ejecta, this process is associated with the contact discontinuity between the two fluids. This discontinuity is unstable, and the resulting instabilities lead to mixing, which while numerical in origin, nevertheless signals contact between the nickel-rich ejecta and helium-rich stellar envelope. In contrast, ablation proceeds through the shock heating of envelope material ahead of the contact discontinuity, and because the shock is more stable, much less mixing is expected where ablation is dominant. The averaged ablated and stripped mass after the initial impact for the different cases studied is shown in Figure 8.

We find that the ablated mass is comparable to the stripped mass for smaller binary separations, and the amount ablated is sensitive to the binary separation dur-

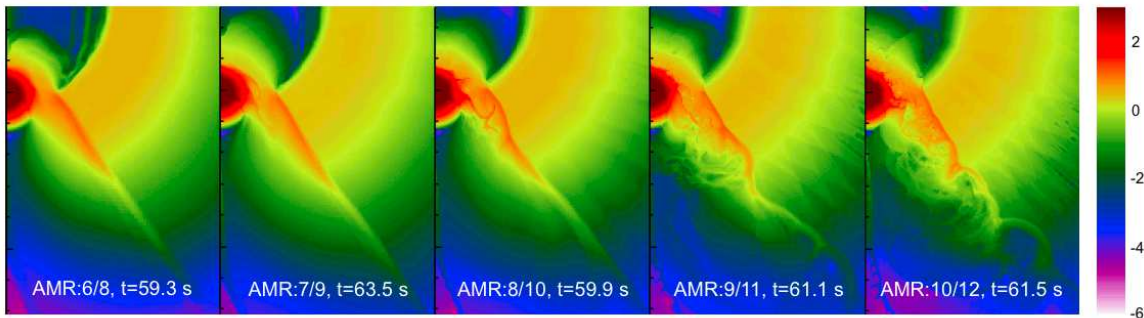


FIG. 6.— The density distribution for model He-WDc with initial binary separation 3×10^{10} cm. Each frame shows the evolution time at around one minute for different AMR levels. The color scale indicates the logarithm of the gas density in g cm^{-3} .

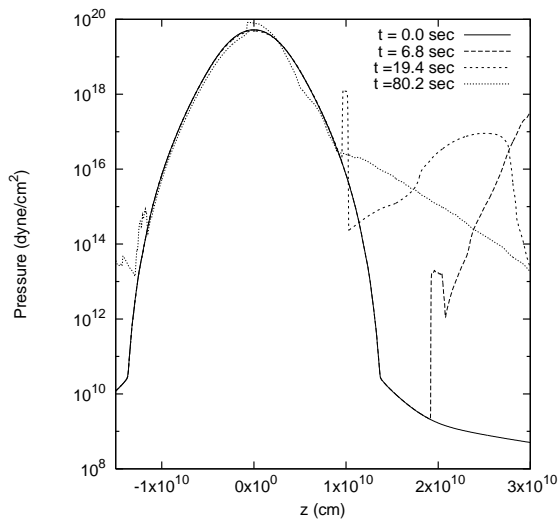


FIG. 7.— Pressure profile along the z -axis at different times for model He-WDc with an initial binary separation of 4×10^{10} cm and 9/11 levels of refinement. The solid line is the original pressure profile before the SN explosion.

ing the initial phase (less than 100 seconds for the case of model He-WDc). The final results suggest that in most cases the amount of stripped mass can be as much as an order of magnitude greater than the ablated mass, depending on the binary separation. The ratio cannot be determined accurately because we did not trace individual fluid elements in these simulations.

A simple analytical method has been used by Meng et al. (2007) to estimate the amount of unbound matter based on conservation of momentum, ignoring the shock dynamics and the effect of ablation. This method yields a shallower power-law slope (-1.9) for unbound mass versus separation than the range that we observe (-3.1 to -4). However, the power-law slopes for unbound mass and kick velocity versus separation found by Meng et al. (2007) are similar to the slopes inferred from the hydrogen-rich stars studied by Marietta et al. (2000). Although the method adopted by Meng et al. (2007) is oversimplified, their result suggests that ablation in main-sequence binary companions may not be as important as for helium-star binary companions. Figure 8 shows that in our simulations the ablated mass corresponds to $\sim 1 - 20\%$ of the total unbound mass, with a greater fraction ablated for smaller orbital separations. Thus, the total momentum imparted to the helium star results from contributions by both direct impact of the

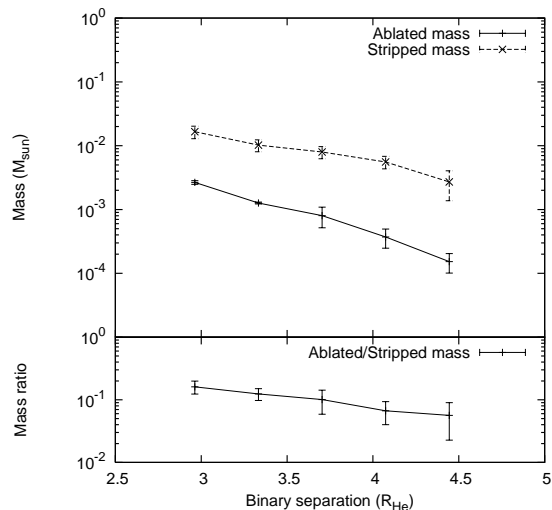


FIG. 8.— Comparison of averaged ablated and stripped helium mass after the initial supernova impact versus the binary separation for model He-WDc (upper panel). Error bars represent the standard deviation during the average time range. The lower panel shows the ratio of ablated to stripped helium mass.

SN ejecta and shock heating, whereas for hydrogen-rich companions the former effect is a more important contributor than the latter. The difference in the relative contribution of these two effects for different types of companion star may explain the difference in the power-law indices for kick velocity.

4.2. Nickel contamination

The companion star can be contaminated by the mixing of supernova ejecta with the helium-rich material in its envelope, perhaps resulting in a detectable enhanced iron abundance after the nickel radioactively decays. Since ^{56}Ni is used as a tracer in our model, we have determined the amount of nickel bound to the remnant helium star. In general, there is a tendency for a higher level of contamination for more massive helium-star companions or for larger orbital separations. In the former case, a massive companion presents a larger cross section for capture of supernova ejecta, whereas in the latter case, the ram pressure from the ejecta is lower for larger binary separations, resulting in a reduction of the amount of contaminated matter that is stripped off. However, the level of contamination in our simulations is highly dependent on the development of small-scale fluid instabilities at multifluid interfaces. Although we find little evidence for a simple relationship between the

amount of contamination and the nature of the helium-star companion or the orbital separation, we can estimate an upper limit on the nickel captured by the helium-rich companion by identifying the ejecta which cannot escape the gravitational potential. This limit is $\sim 5 \times 10^{-4} M_{\odot}$, somewhat smaller than the estimate by Marietta et al. ($\sim 1.5 \times 10^{-3} M_{\odot}$). If the mixing of nickel is only restricted to the envelope, the nickel to helium ratio can be estimated by using the upper limit of nickel contamination and the final envelope mass. We define the core mass for the initial helium-star models by finding the radius at which the second derivative of the density with respect to radius is a maximum; the envelope mass is then the total mass less the core mass. Using this definition, we find that the unbound helium-star material is taken entirely from the envelope. The final envelope mass can thus be obtained from the difference between the initial envelope mass and the final unbound mass in Figure 4 at the separation corresponding to RLOF. We find that the ratio of the upper limit on bound nickel mass to the final envelope helium mass is $\sim 9 - 50 \times 10^{-4}$ for the different helium-star models. This value is substantially higher than the solar ratio of iron abundance to that of hydrogen plus helium (5.1×10^{-4}) found by Anders & Grevesse (1989), suggesting that the abundance of nickel/iron in the remnant helium-star atmosphere should be enhanced relative to normal Population I stars if surface convection is not an important factor.

4.3. Detecting the remnant companion star

After the supernova, the companion star moves with a velocity $\vec{v} \sim \vec{v}_{\text{orb}} + \vec{v}_{\text{kick}}$. The orbital speeds corresponding to the range of binary separations in our simulations are $v_{\text{orb}} \sim 350 - 800 \text{ km s}^{-1}$, while the kick speed $v_{\text{kick}} \sim 30 - 100 \text{ km s}^{-1}$. Thus, the net velocity is primarily determined by the orbital motion for most binary separations. Figure 9 shows the ratio of kick speed to the total speed, assuming that the kick velocity is perpendicular to the orbital velocity. If the mass transfer in the binary system is via RLOF, then the kick contributes little to the total velocity. For very small orbital separations, the kick contributes at most $\sim 10 - 20\%$ of the total.

Based on these observations, we may expect that helium stars with high space motion found to be associated with Type Ia supernova remnants would be evidence for SNe Ia proceeding through the helium-star single-degenerate channel. If such objects are also found to have enhanced iron abundances relative to helium, this evidence would be considerably strengthened. In such cases the relative velocity between the helium star and the centroid of the supernova remnant would place a stronger constraint on the initial binary separation than on the initial helium star’s mass or the white dwarf mass.

5. CONCLUSIONS

We have investigated the impact of SN Ia ejecta on a companion star in the single-degenerate helium-star channel for the short-delay-time population of SN Ia via two-dimensional hydrodynamical simulations using a range of helium-star models and binary orbital separations. Although the general behavior of the tem-

poral evolution is similar to that in previous studies by Marietta et al. (2000) and Pakmor et al. (2008) for

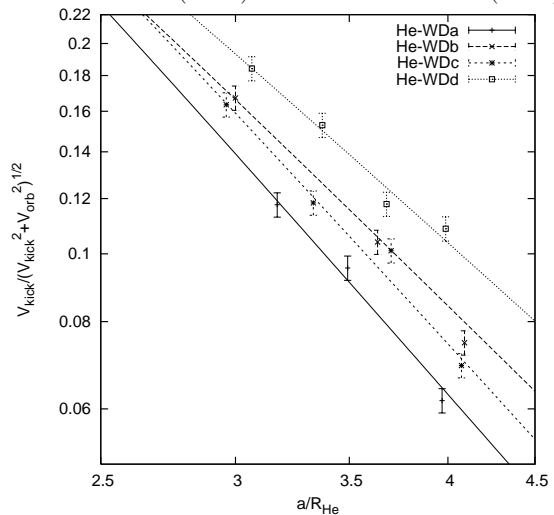


FIG. 9.— The ratio of kick speed to total speed for different helium-star models as a function of initial separation. Lines: from the fitted kick velocity. Data: from the calculated kick velocity. Error bars are based on the 4% error determined in our convergence test. We assume the kick velocity to be perpendicular to the orbital velocity.

main-sequence and red-giant companions, the amount of matter unbound from the helium stars is less than for hydrogen-rich companions. Due to the shorter orbital periods of helium-star progenitor systems, the space motion of the companion star after the explosion is found to be higher. We find a power-law relation between the unbound mass and initial binary separation that is consistent with the previous studies, suggesting that the power-law behavior is not strongly sensitive to the nature of the companion. The kick velocity can also be fitted by a power-law and we conclude that the power-law index may reflect the relative importance of the effect of ablation. An upper limit on the amount of nickel captured by the helium star is found to be $\sim 5 \times 10^{-4} M_{\odot}$. The ratio of nickel to helium abundance may be useful as a diagnostic of such events in future observational studies of SN Ia stellar remnants.

Future work in this area will include relaxing the assumption of axisymmetry to model the mixing of ejecta with the helium star by including the binary orbital motion in three spatial dimensions. Additionally, including radiation transfer within these simulations will allow us to determine how much of the helium is ionized, allowing us to make direct contact with spectroscopic constraints on the presence of helium in these systems.

We thank the anonymous referee for his/her valuable comments and suggestions. The simulations presented here were carried out using the NSF Teragrid’s Ranger system at the Texas Advanced Computing Center under allocation TG-AST040034N. FLASH was developed largely by the DOE-supported ASC/Alliances Center for Astrophysical Thermonuclear Flashes at the University of Chicago. This work was supported, in part, by NSF AST-0703950 to Northwestern University.

REFERENCES

- Anders, E. & Grevesse, N. 1989, *Geochimica et Cosmochimica Acta*, 53, 197
- Aubourg, É., Tojeiro, R., Jimenez, R., Heavens, A., Strauss, M. A., & Spergel, D. N. 2008, *A&A*, 492, 631
- Branch, D. & Tammann, G. A. 1992, *ARA&A*, 30, 359
- Colella, P. & Glaz, H. 1985, *JCP*, 59, 264
- Colella, P. & Woodward, P. R. 1984, *JCP*, 54, 174
- Dessart, L., Burrows, A., Ott, C. D., Livne, E., Yoon, S.-C., & Langer, N. 2006, *ApJ*, 644, 1063
- Domínguez, I., Höflich, P., & Straniero, O. 2001, *ApJ*, 557, 279
- Dubey, A., Reid, L. B., & Fisher, R. 2008, *Physica Scripta*, T132, 014046
- Dwarkadas, V. V. 2000, *ApJ*, 541, 418
- Dwarkadas, V. V. & Chevalier, R. A. 1998, *ApJ*, 497, 807
- Eggleton, P. P. 1971, *MNRAS*, 151, 351
- . 1972, *MNRAS*, 156, 361
- . 1973, *MNRAS*, 163, 279
- Fryxell, B. et al. 2000, *ApJS*, 131, 273
- Goldhaber, G. et al. 2001, *ApJ*, 558, 359
- Hachisu, I., Kato, M., & Nomoto, K. 1996, *ApJL*, 470, L97
- . 1999a, *ApJ*, 522, 487
- . 2008a, *ApJ*, 683, L127
- . 2008b, *ApJ*, 679, 1390
- Hachisu, I., Kato, M., Nomoto, K., & Umeda, H. 1999b, *ApJ*, 519, 314
- Howell, D. A., Sullivan, M., Conley, A., & Carlberg, R. 2007, *ApJ*, 667, L37
- Iben, I. & Tutukov, A. V. 1984, *ApJ*, 54, 335
- Ivanova, N. & Taam, R. E. 2004, *ApJ*, 601, 1058
- Kasen, D. 2010, *ApJ*, 708, 1025
- Knop, R. A. et al. 2003, *ApJ*, 598, 102
- Leonard, D. C. 2007, *ApJ*, 670, 1275
- Mannucci, F. 2005, in *Astronomical Society of the Pacific Conference Series*, Vol. 342, 1604-2004: Supernovae as Cosmological Lighthouses, ed. M. Turatto, S. Benetti, L. Zampieri, & W. Shea, 140
- Mannucci, F., Valle, M. D., & Panagia, N. 2006, *MNRAS*, 370, 773
- Maoz, D. 2008, *MNRAS*, 384, 267
- Marietta, E., Burrows, A., & Fryxell, B. 2000, *ApJS*, 128, 615
- Mattila, S., Lundqvist, P., Sollerman, J., Kozma, C., Baron, E., Fransson, C., Leibundgut, B., & Nomoto, K. 2005, *A&A*, 443, 649
- Meng, X., Chen, X., & Han, Z. 2007, *PASJ*, 59, 835
- Meng, X. & Yang, W. 2009, arXiv:0910.4992
- Napiwotzki, R. et al. 2001, *Astronomische Nachrichten*, 322, 411
- . 2002, *A&A*, 386, 957
- Nelemans, G., Yungelson, L. R., Zwart, S. F. P., & Verbunt, F. 2001, *A&A*, 365, 491
- Nomoto, K. 1982, *ApJ*, 257, 780
- Nomoto, K. & Iben, I. 1985, *ApJ*, 297, 531
- Nomoto, K., Thielemann, F.-K., & Yokoi, K. 1984, *ApJ*, 286, 644
- Pakmor, R., Röpke, F. K., Weiss, A., & Hillebrandt, W. 2008, *A&A*, 489, 943
- Riess, A. G. 1996, Ph.D. thesis, Harvard University
- Scannapieco, E. & Bildsten, L. 2005, *ApJ*, 629, L85
- Timmes, F. X. & Swesty, F. D. 2000, *ApJS*, 126, 501
- Waldman, R., Yungelson, L. R., & Barkat, Z. 2008, in *Astronomical Society of the Pacific Conference Series*, Vol. 391, Hydrogen-Deficient Stars, ed. A. Werner & T. Rauch, 359
- Wang, B., Chen, X., Meng, X., & Han, Z. 2009a, *ApJ*, 701, 1540
- Wang, B. & Han, Z. 2010, *Ap&SS*, in press
- Wang, B., Meng, X., Chen, X., & Han, Z. 2009b, *MNRAS*, 395, 847
- Webbink, R. F. 1984, *ApJ*, 277, 355
- Whelan, J. & Iben, I. 1973, *ApJ*, 186, 1007
- Wickramasinghe, D. T., Hurley, J. R., Ferrario, L., Tout, C. A., & Kiel, P. D. 2009, *Journal of Physics Conference Series*, 172, 012037